



# HHS Public Access

Author manuscript

ACS Chem Biol. Author manuscript; available in PMC 2016 June 19.

Published in final edited form as:

ACS Chem Biol. 2015 June 19; 10(6): 1466–1475. doi:10.1021/cb5010178.

## Optochemical dissection of T-box gene-dependent medial floor plate development

Alexander Y. Payumo<sup>†</sup>, Whitney J. Walker<sup>†</sup>, Lindsey E. McQuade<sup>†,§</sup>, Sayumi Yamazoe<sup>†</sup>, and James K. Chen<sup>\*,†,‡</sup>

<sup>†</sup>Department of Chemical and Systems Biology, Stanford University School of Medicine, Stanford, CA 94305, USA

<sup>‡</sup>Department of Developmental Biology, Stanford University School of Medicine, Stanford, CA 94305, USA

### Abstract

In addition to their cell-autonomous roles in mesoderm development, the zebrafish T-box transcription factors *no tail a (ntla)* and *spadetail (spt/tbx16)* are required for medial floor plate (MFP) formation. Posterior MFP cells are completely absent in zebrafish embryos lacking both Ntla and Spt function, and genetic mosaic analyses have shown that the two T-box genes promote MFP development in a non-cell-autonomous manner. Based on these observations, it has been proposed that Ntla/Spt-dependent mesoderm-derived signals are required for the induction of posterior but not anterior MFP cells. To investigate the mechanisms by which Ntla and Spt regulate MFP development, we have used photoactivatable caged morpholinos (cMOs) to silence these T-box genes with spatiotemporal control. We find that posterior MFP formation requires Ntla or Spt activity during early gastrulation, specifically in lateral margin-derived cells that converge toward the midline during epiboly and somitogenesis. Nodal signaling-dependent MFP specification is maintained in the absence of Ntla and Spt function; however midline cells in *ntla;spt* morphants exhibit aberrant morphogenetic movements, resulting in their anterior mislocalization. Our findings indicate that Ntla and Spt do not differentially regulate MFP induction along the anterior-posterior axis; rather, the T-box genes act redundantly within margin-derived cells to promote the posterior extension of MFP progenitors.

### INTRODUCTION

The medial floor plate (MFP) is a specialized group of cells that occupies the ventral-most region of the vertebrate neural tube.<sup>1</sup> This transient structure acts as a critical organizing center during neural development, secreting signaling molecules such as Sonic hedgehog (Shh) to regulate dorsal-ventral patterning and commissural axon guidance within the spinal

\*Corresponding author. Department of Chemical and Systems Biology, Stanford University School of Medicine, 269 Campus Drive, CCSR 3155, Stanford, CA 94305, USA. Tel: 650-725-3582. Fax: 650-723-2253. jameschen@stanford.edu. .

<sup>§</sup>Present address: Department of Chemistry, University of Illinois, Chicago, IL 60607, USA

#### COMPETING FINANCIAL INTERESTS

The authors declare no competing financial interests.

#### SUPPORTING INFORMATION

This material is available free of charge via the Internet at <http://pubs.acs.org>.

cord.<sup>2–5</sup> How the MFP is specified, organized, and maintained are enduring questions that have inspired divergent models. It was initially proposed that the MFP originates from the neural plate midline, induced by Shh expressed by the underlying notochord.<sup>6</sup> Notochord ablation can disrupt MFP formation in chick embryos, and notochord grafts can promote neural plate differentiation into MFP *in ovo* and *in vitro*. High concentrations of Shh can also induce the expression of MFP markers in avian neural plate explants,<sup>7–9</sup> and mice lacking Shh, the transmembrane receptor Smoothed (Smo), or the transcription factor Gli2 fail to form MFP,<sup>10–13</sup> suggesting a conserved role for notochord- and Hedgehog (Hh) signaling-dependent MFP formation in amniotes.

Subsequent studies in anamniotes such as zebrafish supported an alternative model for MFP ontogeny. Zebrafish with mutations in the T-box gene *no tail-a (ntla)*, an ortholog of *Brachyury*, form the MFP despite a complete absence of notochord cells, and cell lineage analyses indicate that the zebrafish MFP stems from pluripotent precursors located within the dorsal organizer (embryonic shield).<sup>14, 15</sup> Cells specified to become MFP are then inserted into the midline of the neural tube as gastrulation proceeds. Genetic and chemical perturbations have further demonstrated that MFP induction in zebrafish does not require orthologs of Shh (Shha and Shhb), Indian hedgehog (Ihhb), Smo, or Gli2 (Gli2a).<sup>16–20</sup> Rather, MFP development is disrupted in *cyclops (cyc)* and *one-eyed pinhead (oep)* mutants, which lack the Nodal-related-2 (Ndr2) ligand and its receptor teratocarcinoma-derived growth factor-1 (Tdgf1), respectively.<sup>21–26</sup> Both *ndr2* and *tdgf1* are expressed within the shield, and studies using a temperature-sensitive *cyc* mutant have shown that Nodal pathway-dependent MFP induction occurs during early gastrulation.<sup>27</sup> Nodal signaling may act at least in part by suppressing Ntla, since loss of *ntla* function rescues trunk MFP in *cyc* and *oep* mutants.<sup>25, 28</sup> Ndr2 is similarly not required for trunk and tail MFP formation in the absence of a second T-box gene, *spadetail (spt/tbx16)*, which regulates paraxial mesoderm patterning.<sup>29–31</sup>

Despite these disparate models of MFP development, several findings indicate that the mechanisms of MFP formation are more conserved between amniotes and anamniotes than has been previously appreciated. Chick embryos subjected to notochord ablation can eventually form MFP cells after a temporal delay,<sup>32</sup> suggesting that MFP induction involves early, notochord-independent processes. Consistent with this idea, studies of quail-chick chimeras demonstrate that MFP and notochord cells originate from the avian equivalent of the dorsal organizer, Hensen's node, with MFP progenitors inserting into the neural plate as the node regresses caudally.<sup>33</sup> Nodal signaling can also cooperate with Shh to promote MFP marker expression in avian neural plate explants.<sup>34</sup> Conversely, although zebrafish with inactivating Hh pathway mutations can form the MFP, they prematurely lose expression of MFP markers at later developmental stages.<sup>20</sup> Moreover, *cyc* and *oep* mutants gradually acquire MFP cells in a *shha*- and *smo*-dependent manner.<sup>25, 35</sup> Thus, apparent species-specific differences in MFP development may merely reflect varying contributions of Hh and Nodal signaling to MFP specification and maintenance.

Amidst these evolving and converging models, how T-box genes contribute to MFP development has remained a long-standing paradox. The MFP domain is broadened in zebrafish lacking either *ntla* or *spt*, indicating that these transcription factors restrict MFP

fate specification.<sup>14, 28, 31</sup> However, MFP cells are completely missing from the trunks and tails of *ntla*;*spt* mutants, and cell transplantation experiments have demonstrated that the two T-box genes are non-cell-autonomously required for caudal MFP formation.<sup>31</sup> Based on these ostensibly opposing activities, it has been postulated that Ntla and Spt redundantly produce an early inductive signal for MFP specification and act later to restrict MFP cell fates.<sup>31</sup> The loss of posterior MFP in embryos lacking Ntla and Spt function has also been interpreted as evidence for rostrocaudal differences in MFP induction.<sup>31</sup> Reconciling these divergent roles of Ntla and Spt in MFP development has been a challenge, in part due to the constitutive loss of function in their corresponding mutants.

Here we describe our investigations of Ntla/Spt-dependent MFP development using cyclic caged morpholinos (cMOs). These photoactivatable reagents convey spatiotemporal control of gene function, allowing us to examine when and where these T-box genes act to promote posterior MFP patterning. We find that knockdown of Ntla and Spt function in the lateral margins of early gastrulae causes loss of caudal MFP, recapitulating this aspect of the *ntla*;*spt* mutant phenotype. The spatial separation of these targeted cells and MFP progenitors within the dorsal organizer argues against a Ntla/Spt-dependent signal that coincides with MFP induction. Nodal and Hh signaling are correspondingly intact in zebrafish embryos injected with both *ntla* and *spt* MOs, and these double morphants have similar numbers of *shha*-expressing MFP cells as embryos lacking *ntla* function alone. We instead observe that lateral margin-derived cells converge toward the midline during gastrulation and that MFP cells fail to extend caudally in *ntla*;*spt* morphants. Our results support a model in which T-box genes redundantly and non-cell-autonomously promote posterior MFP formation by regulating the morphogenetic movement of progenitor cells.

## METHODS

### Zebrafish husbandry

Adult wildtype zebrafish (*Danio rerio*; AB strain) were obtained from the Zebrafish International Resource Center (ZIRC), and *Tg(-2.4shha-ABC:GFP)* zebrafish were obtained from U. Strähle.<sup>36</sup> All adults were maintained according to standard protocols,<sup>37, 38</sup> and all embryos were obtained by natural matings and cultured at 28.5 °C.

### Morpholino reagents and photoactivatable lineage tracers

Antisense MOs (Gene-Tools) targeting the following genes were microinjected into 1- to 4-cell-stage embryos: *ntla* (5'-GACTTGAGGCAGACATATTTCCGAT-3') and *spt* (5'-CTCTGATAGCCTGCATTATTTAG CC-3'). Each oligonucleotide was injected at a dose of 1.5 ng/embryo, either separately or in combination. A photoactivatable *spt* cMO with the oligonucleotide sequence above was synthesized as described<sup>39</sup> and injected at a dose of 1 ng/embryo when utilized alone or 0.375 ng/embryo when combined with the *ntla* MO.

Caged fluorescein-conjugated dextran (cFD) was synthesized as reported.<sup>40</sup> Caged Q-rhodamine-conjugated dextran (cRD) was similarly prepared with minor modifications. NVOC2-5-carboxy-Q-rhodamine (Sigma-Aldrich) (2.50 mg, 2.68 μmol), *N,N*-diisopropylethylamine (1.40 μL, 8.02 μmol), and *N,N,N',N'*-tetramethyl-O-(*N*-succinimidyl)

uronium tetrafluoroborate (1.00 mg, 3.32  $\mu\text{mol}$ ) were dissolved in DMF (103  $\mu\text{L}$ ), and the solution was stirred at room temperature in the dark for 16 h. The reaction was then partitioned between EtOAc and 10% (w/v) aqueous citric acid, and the organic layer was washed twice with water and brine, dried over anhydrous  $\text{MgSO}_4$ , filtered and concentrated *in vacuo* to afford the NHS ester (1.91 mg, 69%).  $^1\text{H}$  NMR (300 MHz,  $\text{CDCl}_3$ ): 1.96 (m, 4H), 2.63 (m, 4H), 2.99 (br s, 4H), 3.83 (m, 4H), 3.93 (s, 6H), 3.99 (s, 6H), 5.70 (m, 4H), 6.49 (s, 2H), 7.06 (s, 2H), 7.32 (d,  $J = 8.1$  Hz, 1H), 7.76 (s, 2H), 7.82 (br s, 2H), 8.44 (dd,  $J = 8.1, 1.5$  Hz, 1H), 8.85 (d,  $J = 1.5$  Hz, 1H). NVOC-5-carboxy-Q-rhodamine NHS ester (1.91 mg, 1.85  $\mu\text{mol}$ ) was added to a suspension of 10,000-MW aminodextran (3.50 mg, 0.350  $\mu\text{mol}$ ; Life Technologies) in 500  $\mu\text{L}$  of 0.1 M  $\text{Na}_2\text{B}_4\text{O}_7$  buffer (pH 8.5), and the reaction was vortexed in a 1.5-mL microcentrifuge tube overnight. The reaction mixture was added to a Zeba spin desalting column (Thermo Scientific), and the cRD-containing eluent was lyophilized. Both cFD and cRD were injected into 1- to 4-cell stage zebrafish as 0.2% (w/v) aqueous solutions (3 nL/embryo).

### Photoactivation of caged reagents

To globally irradiate pools of zebrafish embryos, a 6-well microplate was mounted onto a mirrored surface and then fixed onto a Vortex-Genie 2 (Scientific Industries). Chorionated embryos were added to a single well filled with E3 medium, agitated with the vortexer on setting 1, and irradiated for 15 minutes with a 365–370 nm LED source (Stanford Photonics). LED current was maintained at 7 A, resulting in a light intensity of 10.6  $\text{mW}/\text{cm}^2$  at the well bottom. For individual, global irradiations, chorionated embryos were arrayed in an agarose template (560- $\mu\text{m}$  x 960- $\mu\text{m}$  wells) filled with E3 medium, oriented with the animal pole facing up. Each embryo was then irradiated for 15 seconds using a Leica DM4500B upright compound microscope equipped with a mercury lamp, an A4 filter (Ex: 360 nm, 40-nm bandpass), and a 20x/0.5 NA water-immersion objective. The light intensity at the focal point was measured to be 410  $\text{mW}/\text{cm}^2$ . For spatially localized uncaging, chorionated shield-stage embryos were positioned in agarose templates and irradiated for 15 seconds using the Leica DM4500B system described above. Using adjustable diaphragms, the irradiation area was limited to either a 100- $\mu\text{m}$ -diameter circular region or a 200- $\mu\text{m}$  x 400- $\mu\text{m}$  rectangular region.

### Whole-mount immunostaining and in situ hybridization

Embryos were fixed at the desired developmental stage in 4% (w/v) paraformaldehyde in PBS and then immunostained as described<sup>41</sup> and imaged with the Leica DM4500B microscope. The following antibodies were used: mouse monoclonal anti-Tbx16 (1:100 dilution, ZIRC, ZDB-ATB-081002-3), rabbit polyclonal anti-Ntla (1:100 dilution),<sup>40</sup> mouse monoclonal anti-fluorescein (1:200 dilution, Roche, 1425320), and rabbit polyclonal anti-fluorescein (1:50 dilution, Molecular Probes, A-889).

Whole-mount *in situ* hybridization of RNA transcripts was performed according to standard protocols.<sup>42</sup> The *ptch2* riboprobe has been previously described.<sup>43</sup> To obtain additional probes, zebrafish cDNA was prepared from RNA extracted from bud-stage (10 hours post fertilization; hpf), 8-somite (13 hpf), and 26-somite (22 hpf) embryos with an RNAqueous-Micro Kit (Ambion) and reverse-transcribed with the SuperScript III First-Strand Synthesis

System (Life Technologies). The following T7 promoter-containing, gene-encoding PCR products were then amplified with the designated primers (T7 sequence underlined): *shhb* (5'-TGAGGGACGGGCAGTGGACA-3' and 5'-CGTAATACGACTCACTATAGGGCGCGGTGA CTGGCGCAAAG-3'), *ndr2* (5'-CTCGGAGTGTTCGGAAAGCA-3' and 5'-CGTAATACGACTCACTATAGGGAGATCGCCACGTAGTGGTTG-3'), *lft2* (5'-CCCGGCTCACATTAAGAGCA-3' and 5'-CGTAATACGACTCACTATAGGGAGCACCTCCACCCAGTAGAT-3'), *tdgf1* (5'-GATCTCCCCTGTTGAACGCA-3' and 5'-CGTAATACGACTCACTATAGGGATGGGCCAAATGGACGACTT-3'), *pitx2a* (5'-CCTCCAGTCCAGAGTCCGTA-3' and 5'-CGTAATACGACTCACTATAGGGTCCATCACAGGATTGGACGC-3'). Riboprobes were *in vitro* transcribed from these templates using a MEGAscript T7 Transcription Kit (Life Technologies), substituting kit nucleotides with a digoxigenin RNA labeling mix (Roche). Embryos were imaged using a Leica M205FA stereomicroscope.

### Time-lapse microscopy

Chorionated, shield-stage embryos were inserted into an agarose template filled with E3 medium, oriented with the shield facing down. Imaging was performed with a Leica DMI6000B inverted compound microscope controlled by MetaMorph software (Molecular Devices). Fluorescent signals were acquired with auto-exposure control to account for progressive photobleaching, and ImageJ software was used to adjust brightness and recursively align stacked images using the StackReg and TurboReg plug-ins.<sup>44</sup>

### Flow cytometry

*Tg(-2.4shha-ABC:GFP)* and wildtype AB zebrafish were crossed, and the resulting embryos were injected with *ntla* and/or *spt* MOs. For each experimental condition, 15 to 20 embryos heterozygous for the GFP reporter were dissociated into single cells as described.<sup>40</sup> The cells were then analyzed on a BD FACSAria sorter equipped with a 100- $\mu$ m nozzle. The population of viable, single zebrafish cells was identified through forward- and side-scatter gating and used to determine the percentage of GFP-positive cells for each sample.

### Quantitative RT-PCR

For each experimental condition, total RNA was isolated from 30 embryos using the RNAqueous-Micro Kit, and 3  $\mu$ g was converted into first-strand cDNA using the SuperScript III First-Strand Synthesis System. The resulting 20- $\mu$ L solution of cDNA was diluted 1:10 with water, and 2  $\mu$ L was used as the template for analysis with *shhb* (Dr03112045\_m1, 4351372) and *eef1a111* (Dr03432748\_m1, 4331182) TaqMan probes (Life Technologies) and a Light Cycler 480II (Roche).

## RESULTS AND DISCUSSION

### Functional validation of *ntla* and *spt* MOs

To facilitate our studies of Ntla/Spt-dependent MFP development, we first investigated the ability of previously reported MOs<sup>41, 45</sup> to recapitulate the *ntla*, *spt*, and *ntla;spt* mutant

phenotypes.<sup>31</sup> Zygotic transcription of *ntla* is initially observed throughout the germ ring at the onset of gastrulation (shield stage, 6 hpf) and becomes restricted to the axial mesoderm and tailbud at later stages.<sup>15</sup> *ntla* mutants correspondingly fail to form the notochord and tail mesoderm and exhibit mispatterned, U-shaped somites.<sup>14</sup> In comparison, *spt* is ubiquitously expressed in sphere-stage (4 hpf) embryos and then becomes localized to the germ ring by 6 hpf.<sup>30</sup> As epiboly proceeds, this T-box gene is excluded from the shield but maintained in the prechordal mesoderm, ventrolateral regions of the gastrula margin, and the paraxial hypoblast. Trunk somites are missing in *spt* mutants, and muscle progenitors mislocalize to the tailbud.<sup>29</sup> In comparison, *ntla*;*spt* mutants are devoid of both trunk and tail mesoderm, indicating that the two T-box genes have synergistic and/or redundant functions.<sup>31</sup> Embryos injected with our *ntla* and *spt* MOs, either individually or in combination, faithfully reproduced these morphological phenotypes (Supplementary Figure 1).

We further confirmed that our *ntla* and *spt* MOs can phenocopy the MFP patterning defects observed in single and double mutants. Wildtype zebrafish and *spt* mutants specifically express *shha* in the notochord and MFP, while *ntla* and *ntla*;*spt* mutants exhibit only *shha*-positive MFP cells since they fail to specify notochord progenitors.<sup>31</sup> We therefore examined the effects of these MOs on *shha* expression using *Tg(-2.4shha-ABC:GFP)* embryos.<sup>36</sup> Consistent with previous mutant analyses,<sup>31</sup> the posterior MFP was disrupted in *ntla*;*spt* morphants (Supplementary Figure 2a). Identical morphant phenotypes were obtained using *shhb* as an alternative, more selective MFP marker (Supplementary Figure 2b).<sup>46</sup> Collectively, these findings validate the *ntla* and *spt* MOs as effective, specific tools for studying the roles of these T-box genes in MFP development.

### MFP defects are evident by late gastrulation in *ntla*;*spt* morphants

To define the developmental stage(s) by which MFP defects occur in the absence of *ntla* and/or *spt* function, we conducted a time-course analysis of *shhb* expression in the corresponding morphants. We found that loss of either T-box gene resulted in the premature appearance of *shhb*-expressing dorsal cells in shield-stage embryos (Figure 1a). Transcription of *shhb* was also initiated early in *ntla*;*spt* morphants, encompassing a broader dorsal domain than that observed in the single morphants. By 90% epiboly (9 hpf), both wildtype and morphant embryos had axial *shhb*-expressing cells continuously spanning the anterior-posterior axis (Figure 1b). Double morphants also exhibited *shhb* expression throughout the germ ring, which coincided with ectopic Hh target gene transcription (*ptch2*) (Supplementary Figure 3). By the end of gastrulation (10 hpf), wildtype and single morphants maintained a continuous domain of axial *shhb*-positive cells along the anterior-posterior axis (Figure 1c); however, the *ntla*;*spt* morphants began to show gaps in *shhb* expression between the tailbud and more anterior midline cells. This discontinuity became significantly more pronounced by the 8-somite stage (13 hpf), at which time the *shhb*-positive cells in double morphants appeared to occupy an expanded anterior domain in comparison to those in wildtype embryos and single morphants (Figure 1d).

### *Ntla* and *Spt* act during early gastrulation to promote MFP development

Since zebrafish lacking *ntla* and *spt* function exhibit defects in *shhb* expression by the end of epiboly, we hypothesized that the two T-box genes redundantly promote posterior MFP

formation during gastrulation. To examine the timing of *ntla* and *spt* action in this process, we explored the application of photoactivatable cMOs. Cyclic cMOs targeting *ntla* or *spt* are effective tools for regulating each gene individually;<sup>39, 45</sup> however, we observed that their combined basal activities caused light-independent mesoderm defects by 24 hpf (A. Payumo and J. Chen, data not shown). This is likely due to the reciprocal regulation of the two genes; *ntla* transcription is significantly diminished in the dorsal side of *spt* mutant gastrulae,<sup>47</sup> and *spt* transcription is partially reduced in the hypoblasts of *ntla* mutants.<sup>30</sup> The *ntla* and *spt* cMO basal activities therefore have synergistic effects on mesoderm development, and further improvements in cMO design will be necessary to realize the full potential of combinatorial applications.

We therefore considered combining the *ntla* MO with a *spt* cMO to achieve a light-dependent transition between *ntla* and *ntla;spt* morphants. Zebrafish embryos injected with the *spt* cMO and cultured in the dark developed normally, whereas global 360-nm irradiation of these embryos at 3 hpf recapitulated the *spt* mutant phenotype (Figure 2a–b). Similarly, co-injection of the *ntla* MO and *spt* cMO without irradiation only resulted in morphological defects associated with loss of *ntla* function, as indicated by the absence of notochord and tail mesoderm and the presence of trunk somites (Figure 2c). Exposure of these *ntla* MO/*spt* cMO-injected embryos to 360-nm light at 3 hpf phenocopied the severe mesodermal deficits observed in *ntla;spt* mutants (Figure 2d).

We next validated the ability of the *spt* cMO to convey spatiotemporal control of Spt protein expression. As determined by whole-mount immunostaining, Spt knockdown was observed when zebrafish embryos were injected with the *spt* cMO, either alone or in combination with the *ntla* MO, and then irradiated at various developmental stages (Supplementary Figure 4a–b). To confirm the ability of the *spt* cMO to induce regiospecific loss of Spt function, we injected caged fluorescein-conjugated dextran (cFD) with or without the *spt* cMO into zebrafish embryos, and then irradiated a circular, 100- $\mu$ m-diameter region within the ventral margin at the shield stage (Supplementary Figure 4c). The embryos were then fixed at the bud stage and immunostained with anti-fluorescein and anti-Spt antibodies. As expected, Spt knockdown coincided with irradiated, fluorescein-positive cells in cFD/*spt* cMO-injected embryos (Supplementary Figure 4d).

We proceeded to use this optochemical approach to characterize the timing by which *ntla* and *spt* redundantly promote MFP formation. We injected embryos with the *ntla* MO and *spt* cMO and globally irradiated them at multiple time points spanning the blastula period (3 hpf) and the end of gastrulation (10 hpf). The embryos were fixed at 24 hpf, and the resulting MFP phenotypes were scored according to the number and distribution of *shhb*-expressing cells (Figure 3a). Class I morphants were defined to have severe mispatterning of the anterior MFP and clear deficits of trunk and posterior MFP, resembling *ntla;spt* mutants; class II morphants exhibited anterior MFP broadening and posterior MFP spanning at least the yolk extension; and class III morphants had normal anterior MFP patterning and posterior MFP continuing beyond the yolk extension.

Reproducing the MFP defects observed in *ntla;spt* mutants required photoactivation of the *spt* cMO in *ntla* morphants by the shield stage (6 hpf), and generating the *ntla;spt* morphant

even one hour later yielded significantly weaker MFP phenotypes (Figure 3b). Since Spt expression begins at 4 hpf, we examined the kinetics of Spt protein turnover in shield-stage embryos upon *spt* cMO uncaging. As determined by whole-mount immunostaining, Spt levels were significantly reduced within one hour, and maximum protein knockdown was achieved within two hours (Supplementary Figure 5). These observations indicate that Ntla and Spt act shortly after their expression domains coalesce to promote MFP development, consistent with their redundant contributions to this process.

### Ntla/Spt activity in the lateral margins promotes MFP development

Ntla and Spt are co-expressed throughout the germ ring at the onset of epiboly, and we therefore sought to determine where they act within the gastrula margin to promote MFP development. We injected embryos with the *ntla* MO and *spt* cMO reagents as before and then irradiated rectangular domains (200  $\mu\text{m}$  x 400  $\mu\text{m}$ ) that encompass dorsal, lateral, or ventral regions of the margin at 6 hpf (Figure 3c). Using the phenotypic classifications described above, we observed that *spt* cMO photoactivation in either of the lateral margins resulted in more severe MFP defects than those induced by targeting the dorsal or ventral domains. Suppressing Spt expression in both lateral margins led to even greater losses of posterior, *shhb*-expressing MFP cells, approaching the deficits observed in *ntla;spt* morphants or upon global *spt* cMO uncaging at 6 hpf (Figure 3d). Since MFP progenitors originate from the shield domain of dorsal margin,<sup>14</sup> these findings support the non-cell-autonomous function of these T-box transcription factors in posterior MFP development.<sup>31</sup>

### Lateral margin-derived cells influence MFP progenitor movement

To better understand how lateral margin-derived cells might influence MFP development at the midline, we examined the relative morphogenetic movements of both cell populations. We injected *Tg(-2.4shha-ABC:GFP)* embryos with caged Q-rhodamine-conjugated dextran (cRD) to enable the simultaneous tracking of optically targeted tissues and GFP-expressing midline cells (notochord and MFP progenitors in wildtype embryos and *spt* morphants; MFP progenitors in *ntla* and *ntla;spt* morphants). Consistent with earlier studies describing convergent-extension movements during zebrafish gastrulation,<sup>48, 49</sup> cells derived from the lateral margin of wildtype, shield-stage embryos converged toward midline populations by early somitogenesis (13 hpf) (Figure 4a). We observed comparable morphogenetic movements in *Tg(-2.4shha-ABC:GFP)* embryos injected with either the *ntla* or *spt* MO, although the midline/lateral margin boundary was less defined in these single morphants (Figure 4b–c). Dorsal convergence of lateral margin-derived cells was also maintained along the anterior-posterior axis of *Tg(-2.4shha-ABC:GFP)* embryos injected with both MOs; however, the posterior domain of GFP-positive MFP precursors was dramatically reduced and the anterior domain was correspondingly expanded (Figure 4d).

Time-lapse imaging of *Tg(-2.4shha-ABC:GFP) ntle;spt* morphants further established that GFP-positive MFP precursors become excluded from the posterior midline as gastrulation is completed (Supplementary Movie 1). These GFP-labeled cells are then increasingly limited to anterior regions as somitogenesis proceeds. In contrast, the corresponding MFP progenitors in *Tg(-2.4shha-ABC:GFP) ntle* morphants span the entire midline by the end of epiboly and throughout somitogenesis. These observations suggest that *ntla*- and *spt*-

expressing cells within the lateral margin converge toward MFP progenitors by late gastrulation and promote either the posterior extension or maintenance of this midline population.

To distinguish between these two possibilities, we next investigated whether the posterior exclusion in *ntla;spt* morphants is specific to MFP progenitors or a more general effect on midline cells. We injected wildtype embryos with cFD and uncaged the lineage tracer within the shield at 6 hpf, using a circular 100- $\mu$ m-diameter area of irradiation. By the end of gastrulation, the fluorescein-positive, shield-derived cells were distributed along the entire anterior-posterior axis of the midline, as demarcated by Ntla expression (Supplementary Figure 6). However, when these lineage tracing studies were conducted in *ntla;spt* morphants, no fluorescein-positive cells were observed in the posterior midline, and they instead populated anterior regions in greater numbers. Thus, loss of Ntla and Spt function leads to midline morphogenetic defects that affect shield-derived cells irrespective of fate choice.

### Nodal signaling is maintained in the absence of Ntla and Spt

Our findings indicate that Ntla and Spt act within the lateral margins of early gastrulae to establish conditions required for proper MFP morphogenesis at later stages. This model counters earlier suggestions that the two T-box genes act redundantly and non-cell-autonomously to induce MFP specification, as lateral margin-derived cells converge upon the midline only after Nodal signaling-dependent MFP specification has occurred within the shield. To investigate these differing models further, we compared Nodal pathway activities in wildtype embryos and those lacking Ntla and/or Spt function. Dorsal expression of the ligand *ndr2* and co-receptor *tdgf1* was maintained in single and double morphants during gastrulation, the time by which Nodal signaling induces MFP cell fates (Figure 5a–b). Accordingly, the Nodal targets *paired-like homeodomain 2a* (*pitx2a*)<sup>50</sup> and *lefty2* (*lft2*)<sup>51</sup> were transcribed in midline cells under all experimental conditions (Figure 5c–d). Consistent with the ectopic expression of MFP marker *shhb* in *ntla;spt* morphants, we also observed *ndr2*, *tdgf1*, *pitx2a*, and *lft2* transcription in ventrolateral regions of the margin, indicating that Nodal signaling is actually expanded in embryos lacking Ntla and Spt function.

If a defect in cell movement rather fate specification is the primary cause for posterior MFP loss in *ntla;spt* mutants and morphants, these embryos should have a similar number of MFP progenitors as their wildtype and single-morphant counterparts. We therefore analyzed *shhb* transcript levels by quantitative RT-PCR at 22 hpf, by which time the double morphants are clearly devoid of posterior MFP cells. Double morphants actually exhibited a slight increase in *shhb* expression levels in comparison to the other experimental conditions (Figure 6a), perhaps reflecting the broadened anterior domain of *shhb* transcription in these embryos. We also used flow cytometry to quantify the number of GFP-positive MFP cells in 22-hpf *Tg(-2.4shha-ABC:GFP)* zebrafish injected previously with either the *ntla* MO or a combination of *ntla* and *spt* MOs. Corroborating our analyses of T-box gene-dependent *shhb* expression, *Tg(-2.4shha-ABC:GFP)* embryos lacking Ntla and Spt function had a slightly higher percentage of GFP-positive cells than *ntla* morphants at 22 hpf (Figure 6b), despite the absence of posterior MFP in double morphants.

## A new model for Ntla/Spt-dependent MFP development

Taken together, our studies establish a spatiotemporal framework for Ntla- and Spt-dependent MFP development, addressing many of the questions that have defied conventional genetic analyses. First, we observe that loss of these T-box genes, either alone or in combination, activates dorsal expression of the MFP marker *shhb* in shield-stage embryos, and *shhb* is ectopically transcribed in the germ ring of double morphants as gastrulation progresses. RT-PCR quantification of *shhb* transcripts and flow cytometric analyses of *Tg(-2.4shha-ABC:GFP)* zebrafish further reveal that the number of MFP cells at later developmental stages is not reduced in zebrafish lacking both T-box genes. In fact, the total MFP population is moderately expanded in comparison to wildtype and single-morphant embryos. These results suggest that the actions of Ntla and Spt on MFP induction are primarily repressive in nature and that the transcription factors are dispensable for MFP maintenance.

Second, the conditionality afforded by cMOs has enabled us to pinpoint the timing and location of Ntla/Spt action. By optochemically generating *ntla;spt* morphants, we have established that the two T-box genes function redundantly during early gastrulation to promote posterior MFP development. Although Nodal signaling-dependent MFP induction within the dorsal organizer also occurs at this time,<sup>27</sup> our studies suggest that the roles of Ntla and Spt in posterior MFP formation are unrelated to this process. Nodal signaling is maintained in *ntla;spt* morphants, and lateral margin-specific knockdown of both T-box genes is sufficient to cause posterior MFP loss. The co-transcription of *ntla* and *spt* in ventrolateral regions of gastrula margin contrasts their spatial segregation within the dorsal mesoderm, where they contribute to the chordamesoderm and prechordal plate, respectively.<sup>15, 30</sup> The lateral margins are therefore plausible sites of redundant Ntla and Spt function; however, their distal relationship to the shield at the time of MFP induction would seemingly require a long-range or relayed inductive signal.

Our findings support an alternative model, in which cells derived from the lateral margin influence the morphogenetic movements of MFP progenitors at later stages (Figure 7). In accord with earlier reports,<sup>48, 49</sup> we find that these cells converge toward the midline during epiboly, and by the end of gastrulation they flank cells fated to become MFP. This is the same time by which posterior deficits in *shha*- and *shhb*-expressing MFP precursors are first observed in *ntla;spt* morphants, eventually leading to a complete loss of MFP progenitors in posterior regions and their anterior expansion. Our cell lineage tracing studies further demonstrate that the *ntla;spt* morphant phenotype is not specific to MFP cells but rather reflects a general exclusion of shield-derived cells from the posterior midline. Our results therefore suggest that loss of Ntla and Spt causes a defect in cell movement rather than MFP specification or maintenance. Consistent with this idea, *ntla;spt* morphants are competent for Nodal and Hh signaling and have comparable if not larger numbers of MFP cells in comparison to wildtype embryos. Our observations also raise the possibility that morphogenetic defects might contribute to other MFP phenotypes with anterior-posterior asymmetries, such as the regiospecific rescue of MFP cells in *cyc;ntla* and *cyc;spt* mutants<sup>28, 31</sup>

How lateral margin-derived cells might control MFP morphogenesis remains to be elucidated. One possibility is that they provide a signal required for posterior extension of the midline. Alternatively, loss of *Ntla* and *Spt* activity could alter the morphogenetic and/or adhesive properties of these cells, thereby disrupting their biophysical interactions with midline populations. In this context, it is notable that lateral margin-derived cells establish a less defined boundary with midline tissues in single *ntla* and *spt* morphants, and these cells even appear to displace posterior midline cells in double morphants. Such altered cellular interactions could result at least in part from the ventrolateral expansion of Nodal and Hh signaling when both T-box genes are silenced. Defining the *Ntla/Spt*-dependent transcriptome within the lateral margins, perhaps by integrating photoactivatable cMOs with other technologies,<sup>40</sup> will be an important next step toward deconstructing this process.

## Supplementary Material

Refer to Web version on PubMed Central for supplementary material.

## ACKNOWLEDGEMENTS

We thank U. Strähle for *Tg(-2.Ashha-ABC:GFP)* zebrafish and C. Crumpton, B. Gomez, and O. Herman of the Stanford Shared FACS Facility for technical assistance with flow cytometry. This work was supported by the NIH (DP1 HD075622 and R01 GM087292 to J.K.C.), an A. P. Giannini Foundation Fellowship for Medical Research (L.E.M.), and a Japan Society for the Promotion of Science Fellowship (S.Y.).

## REFERENCES

1. Placzek M, Briscoe J. The floor plate: multiple cells, multiple signals. *Nat. Rev. Neurosci.* 2005; 6:230–240. [PubMed: 15738958]
2. Placzek M, Yamada T, Tessier-Lavigne M, Jessell T, Dodd J. Control of dorsoventral pattern in vertebrate neural development: induction and polarizing properties of the floor plate. *Development.* 1991; (Suppl 2):105–122. [PubMed: 1842349]
3. Echelard Y, Epstein DJ, St-Jacques B, Shen L, Mohler J, McMahon JA, McMahon AP. Sonic hedgehog, a member of a family of putative signaling molecules, is implicated in the regulation of CNS polarity. *Cell.* 1993; 75:1417–1430. [PubMed: 7916661]
4. Kennedy TE, Serafini T, de la Torre JR, Tessier-Lavigne M. Netrins are diffusible chemotropic factors for commissural axons in the embryonic spinal cord. *Cell.* 1994; 78:425–435. [PubMed: 8062385]
5. Serafini T, Kennedy TE, Galko MJ, Mirzayan C, Jessell TM, Tessier-Lavigne M. The netrins define a family of axon outgrowth-promoting proteins homologous to *C. elegans* UNC-6. *Cell.* 1994; 78:409–424. [PubMed: 8062384]
6. Placzek M, Tessier-Lavigne M, Yamada T, Jessell T, Dodd J. Mesodermal control of neural cell identity: floor plate induction by the notochord. *Science.* 1990; 250:985–988. [PubMed: 2237443]
7. Roelink H, Augsburger A, Heemskerk J, Korzh V, Norlin S, Ruiz i Altaba A, Tanabe Y, Placzek M, Edlund T, Jessell TM, et al. Floor plate and motor neuron induction by *vhh-1*, a vertebrate homolog of hedgehog expressed by the notochord. *Cell.* 1994; 76:761–775. [PubMed: 8124714]
8. Roelink H, Porter JA, Chiang C, Tanabe Y, Chang DT, Beachy PA, Jessell TM. Floor plate and motor neuron induction by different concentrations of the amino-terminal cleavage product of sonic hedgehog autoproteolysis. *Cell.* 1995; 81:445–455. [PubMed: 7736596]
9. Marti E, Bumcrot DA, Takada R, McMahon AP. Requirement of 19K form of Sonic hedgehog for induction of distinct ventral cell types in CNS explants. *Nature.* 1995; 375:322–325. [PubMed: 7753196]

10. Chiang C, Litingtung Y, Lee E, Young KE, Corden JL, Westphal H, Beachy PA. Cyclopia and defective axial patterning in mice lacking Sonic hedgehog gene function. *Nature*. 1996; 383:407–413. [PubMed: 8837770]
11. Matisse MP, Epstein DJ, Park HL, Platt KA, Joyner AL. Gli2 is required for induction of floor plate and adjacent cells, but not most ventral neurons in the mouse central nervous system. *Development*. 1998; 125:2759–2770. [PubMed: 9655799]
12. Wijgerde M, McMahon JA, Rule M, McMahon AP. A direct requirement for Hedgehog signaling for normal specification of all ventral progenitor domains in the presumptive mammalian spinal cord. *Genes Dev*. 2002; 16:2849–2864. [PubMed: 12435628]
13. Ding Q, Motoyama J, Gasca S, Mo R, Sasaki H, Rossant J, Hui CC. Diminished Sonic hedgehog signaling and lack of floor plate differentiation in Gli2 mutant mice. *Development*. 1998; 125:2533–2543. [PubMed: 9636069]
14. Halpern ME, Ho RK, Walker C, Kimmel CB. Induction of muscle pioneers and floor plate is distinguished by the zebrafish no tail mutation. *Cell*. 1993; 75:99–111. [PubMed: 8402905]
15. Schulte-Merker S, van Eeden FJ, Halpern ME, Kimmel CB, Nusslein-Volhard C. no tail (ntl) is the zebrafish homologue of the mouse T (Brachyury) gene. *Development*. 1994; 120:1009–1015. [PubMed: 7600949]
16. Schauerte HE, van Eeden FJ, Fricke C, Odenthal J, Strahle U, Haffter P. Sonic hedgehog is not required for the induction of medial floor plate cells in the zebrafish. *Development*. 1998; 125:2983–2993. [PubMed: 9655820]
17. Odenthal J, van Eeden FJ, Haffter P, Ingham PW, Nusslein-Volhard C. Two distinct cell populations in the floor plate of the zebrafish are induced by different pathways. *Dev. Biol*. 2000; 219:350–363. [PubMed: 10694427]
18. Etheridge LA, Wu T, Liang JO, Ekker SC, Halpern ME. Floor plate develops upon depletion of tiggly-winkle and sonic hedgehog. *Genesis*. 2001; 30:164–169. [PubMed: 11477699]
19. Lewis KE, Eisen JS. Hedgehog signaling is required for primary motoneuron induction in zebrafish. *Development*. 2001; 128:3485–3495. [PubMed: 11566854]
20. Chen W, Burgess S, Hopkins N. Analysis of the zebrafish smoothed mutant reveals conserved and divergent functions of hedgehog activity. *Development*. 2001; 128:2385–2396. [PubMed: 11493557]
21. Hatta K, Kimmel CB, Ho RK, Walker C. The cyclops mutation blocks specification of the floor plate of the zebrafish central nervous system. *Nature*. 1991; 350:339–341. [PubMed: 2008211]
22. Rebagliati MR, Toyama R, Haffter P, Dawid IB. cyclops encodes a nodal-related factor involved in midline signaling. *Proc. Natl. Acad. Sci. U. S. A*. 1998; 95:9932–9937. [PubMed: 9707578]
23. Feldman B, Gates MA, Egan ES, Dougan ST, Rennebeck G, Sirotkin HI, Schier AF, Talbot WS. Zebrafish organizer development and germ-layer formation require nodal-related signals. *Nature*. 1998; 395:181–185. [PubMed: 9744277]
24. Schier AF, Neuhauss SC, Helde KA, Talbot WS, Driever W. The one-eyed pinhead gene functions in mesoderm and endoderm formation in zebrafish and interacts with no tail. *Development*. 1997; 124:327–342. [PubMed: 9053309]
25. Strahle U, Jesuthasan S, Blader P, Garcia-Villalba P, Hatta K, Ingham PW. one-eyed pinhead is required for development of the ventral midline of the zebrafish (*Danio rerio*) neural tube. *Genes Funct*. 1997; 1:131–148. [PubMed: 9680314]
26. Zhang J, Talbot WS, Schier AF. Positional cloning identifies zebrafish one-eyed pinhead as a permissive EGF-related ligand required during gastrulation. *Cell*. 1998; 92:241–251. [PubMed: 9458048]
27. Tian J, Yam C, Balasundaram G, Wang H, Gore A, Sampath K. A temperature-sensitive mutation in the nodal-related gene cyclops reveals that the floor plate is induced during gastrulation in zebrafish. *Development*. 2003; 130:3331–3342. [PubMed: 12783802]
28. Halpern ME, Hatta K, Amacher SL, Talbot WS, Yan YL, Thisse B, Thisse C, Postlethwait JH, Kimmel CB. Genetic interactions in zebrafish midline development. *Dev. Biol*. 1997; 187:154–170. [PubMed: 9242414]
29. Ho RK, Kane DA. Cell-autonomous action of zebrafish spt-1 mutation in specific mesodermal precursors. *Nature*. 1990; 348:728–730. [PubMed: 2259382]

30. Griffin KJ, Amacher SL, Kimmel CB, Kimelman D. Molecular identification of spadetail: regulation of zebrafish trunk and tail mesoderm formation by T-box genes. *Development*. 1998; 125:3379–3388. [PubMed: 9693141]
31. Amacher SL, Draper BW, Summers BR, Kimmel CB. The zebrafish T-box genes no tail and spadetail are required for development of trunk and tail mesoderm and medial floor plate. *Development*. 2002; 129:3311–3323. [PubMed: 12091302]
32. Artinger KB, Bronner-Fraser M. Delayed formation of the floor plate after ablation of the avian notochord. *Neuron*. 1993; 11:1147–1161. [PubMed: 8274280]
33. Schoenwolf GC, Bortier H, Vakaet L. Fate mapping the avian neural plate with quail/chick chimeras: origin of prospective median wedge cells. *J. Exp. Zool.* 1989; 249:271–278. [PubMed: 2708947]
34. Patten I, Kulesa P, Shen MM, Fraser S, Placzek M. Distinct modes of floor plate induction in the chick embryo. *Development*. 2003; 130:4809–4821. [PubMed: 12917296]
35. Albert S, Muller F, Fischer N, Biellmann D, Neumann C, Blader P, Strahle U. Cyclops-independent floor plate differentiation in zebrafish embryos. *Dev. Dyn.* 2003; 226:59–66. [PubMed: 12508225]
36. Ertzter R, Muller F, Hadzhiev Y, Rathnam S, Fischer N, Rastegar S, Strahle U. Cooperation of sonic hedgehog enhancers in midline expression. *Dev. Biol.* 2007; 301:578–589. [PubMed: 17157288]
37. Kimmel CB, Ballard WW, Kimmel SR, Ullmann B, Schilling TF. Stages of embryonic development of the zebrafish. *Dev. Dyn.* 1995; 203:253–310. [PubMed: 8589427]
38. Westerfield, M. *The Zebrafish Book*. University of Oregon Press; Oregon: 1995.
39. Yamazoe S, Shestopalov IA, Provost E, Leach SD, Chen JK. Cyclic caged morpholinos: conformationally gated probes of embryonic gene function. *Angew. Chem. Int. Ed. Engl.* 2012; 51:6908–6911. [PubMed: 22689470]
40. Shestopalov IA, Pitt CL, Chen JK. Spatiotemporal resolution of the Ntla transcriptome in axial mesoderm development. *Nat. Chem. Biol.* 2012; 8:270–276. [PubMed: 22286130]
41. Shestopalov IA, Sinha S, Chen JK. Light-controlled gene silencing in zebrafish embryos. *Nat. Chem. Biol.* 2007; 3:650–651. [PubMed: 17717538]
42. Thisse C, Thisse B. High-resolution in situ hybridization to whole-mount zebrafish embryos. *Nat. Protoc.* 2008; 3:59–69. [PubMed: 18193022]
43. Concordet JP, Lewis KE, Moore JW, Goodrich LV, Johnson RL, Scott MP, Ingham PW. Spatial regulation of a zebrafish patched homologue reflects the roles of sonic hedgehog and protein kinase A in neural tube and somite patterning. *Development*. 1996; 122:2835–2846. [PubMed: 8787757]
44. Thevenaz P, Ruttimann UE, Unser M. A pyramid approach to subpixel registration based on intensity. *IEEE Trans. Image Process.* 1998; 7:27–41. [PubMed: 18267377]
45. Yamazoe S, Liu Q, McQuade LE, Deiters A, Chen JK. Sequential gene silencing using wavelength-selective caged morpholino oligonucleotides. *Angew. Chem. Int. Ed. Engl.* 2014; 53:10114–10118. [PubMed: 25130695]
46. Ekker SC, Ungar AR, Greenstein P, von Kessler DP, Porter JA, Moon RT, Beachy PA. Patterning activities of vertebrate hedgehog proteins in the developing eye and brain. *Curr. Biol.* 1995; 5:944–955. [PubMed: 7583153]
47. Warga RM, Mueller RL, Ho RK, Kane DA. Zebrafish Tbx16 regulates intermediate mesoderm cell fate by attenuating Fgf activity. *Dev. Biol.* 2013; 383:75–89. [PubMed: 24008197]
48. Jessen JR, Topczewski J, Bingham S, Sepich DS, Marlow F, Chandrasekhar A, Solnica-Krezel L. Zebrafish trilobite identifies new roles for Strabismus in gastrulation and neuronal movements. *Nat. Cell Biol.* 2002; 4:610–615. [PubMed: 12105418]
49. Myers DC, Sepich DS, Solnica-Krezel L. Convergence and extension in vertebrate gastrulae: cell movements according to or in search of identity? *Trends Genet.* 2002; 18:447–455. [PubMed: 12175805]
50. Bennett JT, Joubin K, Cheng S, Aanstad P, Herwig R, Clark M, Lehrach H, Schier AF. Nodal signaling activates differentiation genes during zebrafish gastrulation. *Dev. Biol.* 2007; 304:525–540. [PubMed: 17306247]

51. Dickmeis T, Aanstad P, Clark M, Fischer N, Herwig R, Mourrain P, Blader P, Rosa F, Lehrach H, Strahle U. Identification of nodal signaling targets by array analysis of induced complex probes. *Dev. Dyn.* 2001; 222:571–580. [PubMed: 11748827]

Author Manuscript

Author Manuscript

Author Manuscript

Author Manuscript

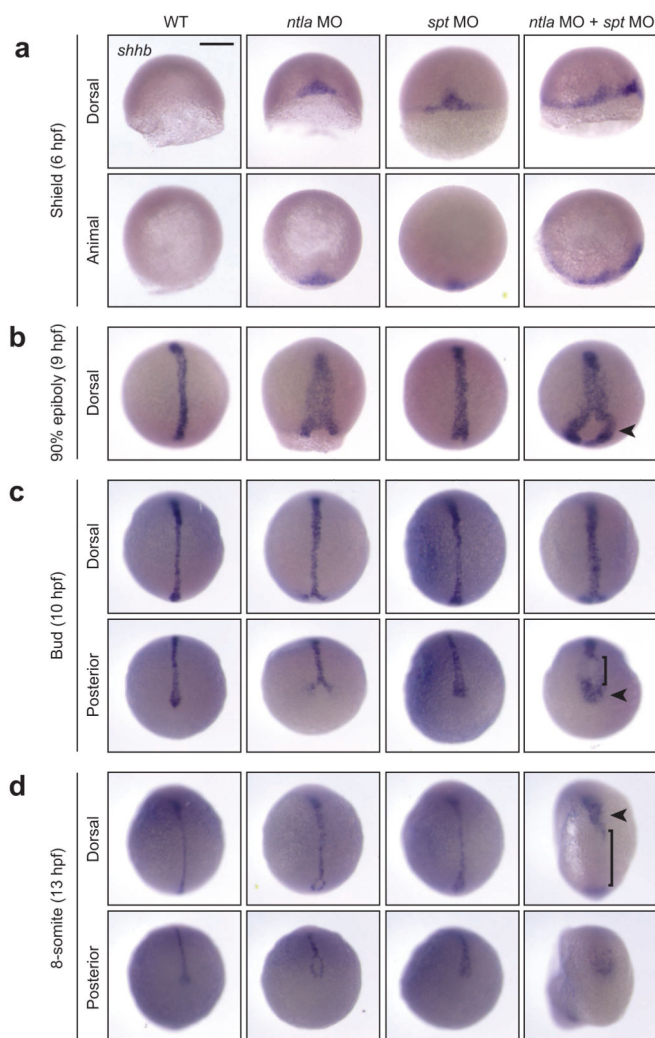


**Figure 1. MFP defects are evident in zebrafish gastrulae lacking *Ntla* and *Spt* function**  
 Expression of the MFP marker *shhb* in wildtype embryos and those without *Ntla* and/or *Spt* function at (a) 6 hpf, (b) 9 hpf, (c) 10 hpf, and (d) 13 hpf. Brackets demarcate posterior regions lacking *shhb*-expressing MFP progenitors, and arrowheads label ectopic *shhb*-positive cells in the germ ring (9 hpf), tailbud (10 hpf), and anterior midline (13 hpf). Embryo orientations: dorsal view, anterior up or posterior view, dorsal up. Scale bar: 200  $\mu$ m.

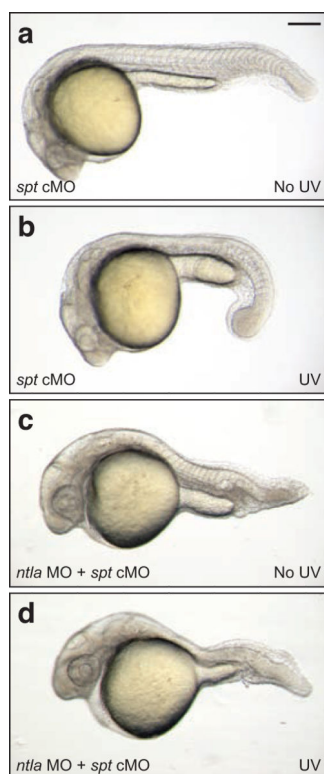


**Figure 2. Optochemical control of Spt function**

Morphological phenotypes observed in zebrafish embryos injected with the *spt* cMO, either alone (a–b) or in combination with a *ntla* MO (c–d). Non-irradiated embryos exhibited wildtype (a) and *ntla* mutant (c) patterning, whereas those subjected to global, 360-nm irradiation at 3 hpf recapitulated *spt* (b) and *ntla*;*spt* (d) mutant defects. 24-hpf embryos are shown in lateral view, anterior left. Scale bar: 200  $\mu$ m.

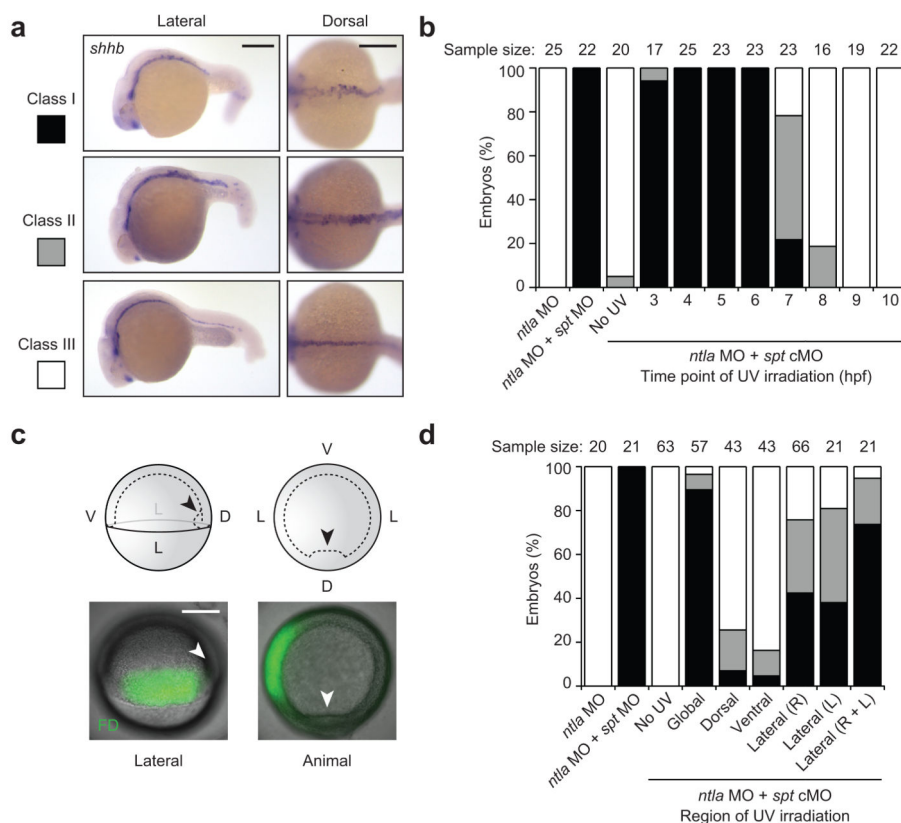


### Figure 3. Spatiotemporal analysis of Ntla/Spt-dependent MFP development

(a) Classification of MFP patterning phenotypes, as determined by *shhb* expression. 24-hpf embryos are shown in lateral view, anterior left or dorsal view, anterior left. (b) Phenotypic distributions for embryos injected with the indicated oligonucleotides and either cultured in the dark or globally irradiated at the designated time points. (c) Regiospecific irradiation of the germ ring in 6-hpf embryos, as illustrated by cFD photoactivation within the lateral left margin. Graphical depictions and overlaid brightfield and fluorescence micrographs of an irradiated embryo are shown. Dorsal (D), ventral (R), and lateral (L) regions of the germ ring are labeled, and arrowheads denote the shield. Embryo orientations: lateral view, dorsal right or animal pole view, dorsal down. (d) Phenotypic distributions for embryos injected with the indicated oligonucleotides and either cultured in the dark or irradiated in the designated manner at 6 hpf. Scale bars: 200  $\mu$ m.

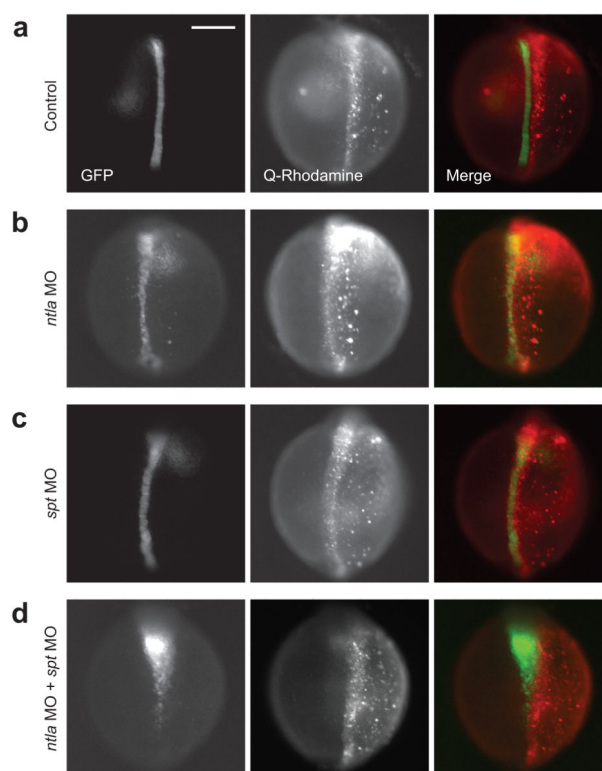


**Figure 4. Convergence of lateral margin-derived cells to the midline**

Morphogenetic movement of cells originating from the right lateral margin, as determined by injecting *Tg(-2.4shha-ABC:GFP)* embryos with cRD and regiospecifically irradiating the germ ring at 6 hpf. Relative positions of the red-fluorescent, lateral margin-derived cells and the GFP-positive midline at 13 hpf are shown for control embryos (a) and those without Ntla and/or Spt function (b–d). Embryo orientations: dorsal view, anterior up. Scale bar: 200  $\mu$ m.

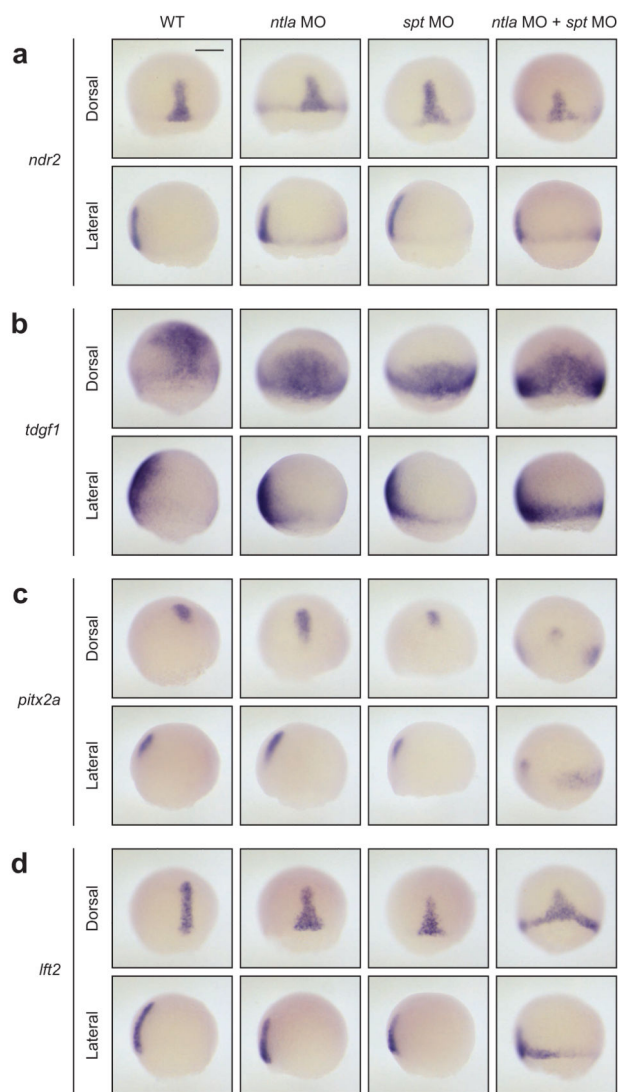


**Figure 5. Nodal signaling is maintained in zebrafish gastrulae lacking Ntla and Spt function**  
 Expression of the Nodal signaling components (*ndr2* and *tdgf1*; a–b) and transcriptional targets (*pitx2a* and *lft2*; c–d) in wildtype embryos and those without Ntla and/or Spt function. Embryos at 75% epiboly are shown in dorsal view, anterior up or lateral view, anterior up. Scale bar: 200  $\mu$ m.

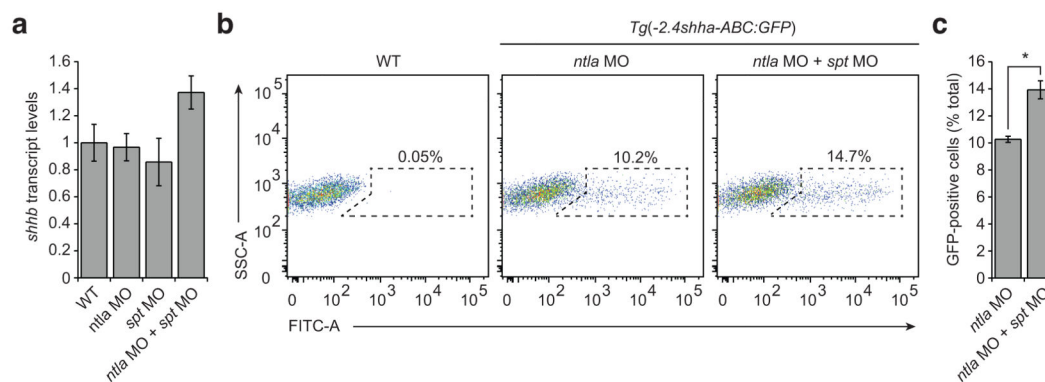


**Figure 6. MFP cell number is conserved in the absence of Ntla and Spt function**

(a) Relative *shhb* transcript levels in 22-hpf wildtype embryos and those without Ntla and/or Spt function, normalized with respect to *efl1a111* expression. (b) Representative flow cytometry scatter plots identifying GFP-positive MFP cells in *Tg(-2.4shha-ABC:GFP)* embryos injected with a *ntla* MO or a mixture of *ntla* and *spt* MOs. (c) Quantification of GFP-positive MFP cells. Data are the average of triplicate samples  $\pm$  s.e.m., and the asterisk indicates  $P < 0.01$ .

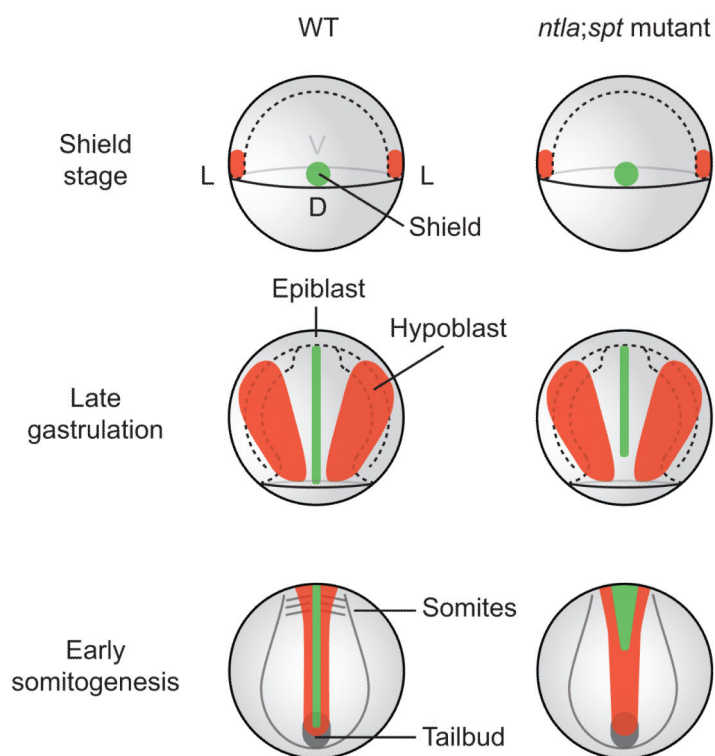


**Figure 7. A model for T-box gene-dependent MFP patterning**

Cells derived from the lateral margins (red) converge to flank the midline (green) in zebrafish embryos, promoting the extension of MFP progenitors along anterior-posterior axis. Loss of *Ntla* and *Spt* function in these cells alters their interactions with midline populations, leading to the anterior mislocalization of MFP progenitors. Dorsal (D), ventral (V), and lateral (L) regions of the margin and selected embryonic structures are labeled.